Received: 8 August 2020 | Accepted: 7 January 2021

DOI: 10.1111/jth.15252

ORIGINAL ARTICLE

Photobiomodulation therapy for thrombocytopenia by upregulating thrombopoietin expression via the ROS-dependent Src/ERK/STAT3 signaling pathway

Qiuhong Wang[1,2] | Haocai Chang[1,2] | Qi Shen[1,2] | Yonghua Li[1,2] | Da Xing[1,2]

[1]MOE Key Laboratory of Laser Life Science & Institute of Laser Life Science, College of Biophotonics, South China Normal University, Guangzhou, China

[2]Guangdong Provincial Key Laboratory of Laser Life Science, College of Biophotonics, South China Normal University, Guangzhou, China

Correspondence
Da Xing, MOE Key Laboratory of Laser Life Science & Institute of Laser Life Science, College of Biophotonics, South China Normal University, 55 Zhongshan Avenue West, Tianhe District, Guangzhou 510631, China.
Email: xingda@scnu.edu.cn

Funding information
The Science and Technology Program of Guangzhou, Grant/Award Number: 2019050001; National Natural Science Foundation of China, Grant/Award Number: 61361160414, 62005085 and 31470072; The science and technology project of Guangzhou, Grant/Award Number: 201805010002; The Science and Technology Planning Project of Guangdong Province (Guangdong-Hong Kong Joint Innovation Project), China, Grant/Award Number: 2014B050504009

Abstract

Background: Chemotherapy-induced thrombocytopenia (CIT) can increase the risk of bleeding, which may delay or prevent the administration of anticancer treatment schedules. Photobiomodulation therapy (PBMT), a non-invasive physical treatment, has been proposed to improve thrombocytopenia; however, its underlying regulatory mechanism is not fully understood.

Objective: To further investigate the mechanism of thrombopoietin (TPO) in megakaryocytopoiesis and thrombopoiesis.

Methods: Multiple approaches such as western blotting, cell transfection, flow cytometry, and animal studies were utilized to explore the effect and mechanism of PBMT on thrombopoiesis.

Results: PBMT prevented a severe drop in platelet count by increasing platelet production, and then ameliorated CIT. Mechanistically, PBMT significantly upregulated hepatic TPO expression in a thrombocytopenic mouse model, which promoted megakaryocytopoiesis and thrombopoiesis. The levels of TPO mRNA and protein increased by PBMT via the Src/ERK/STAT3 signaling pathway in hepatic cells. Furthermore, the generation of the reactive oxygen species was responsible for PBMT-induced activation of Src and its downstream target effects.

Conclusions: Our research suggests that PBMT is a promising therapeutic strategy for the treatment of CIT.

KEYWORDS
megakaryocytes, photobiomodulation therapy, platelets, thrombocytopenia, thrombopoietin

1 | INTRODUCTION

Thrombocytopenia is a common complication in cancer patients receiving chemotherapy, and leads to life-threatening consequences.[1] Myelosuppression is considered to be the main cause of chemotherapy-induced thrombocytopenia (CIT), which can result in different degrees of blood cytopenias.[2,3] In addition to increasing the risk of bleeding, CIT may also limit the dose intensity of chemotherapy and the effectiveness of cancer treatment. In recent decades, considerable progress has been made in the development of therapeutic agents for the treatment of CIT.[4] Thrombopoietic agents, including recombinant human interleukin-11 (rhIL-11), recombinant human thrombopoietin (rhTPO), and thrombopoietin (TPO) receptor agonists eltrombopag or romiplostim,[5] can increase

Manuscript handled by: Katsue Suzuki-Inoue

Final decision: Katsue Suzuki-Inoue, 07 January 2021

platelet production by stimulating megakaryocyte maturation, but these are often accompanied by serious side effects such as fatigue, fever, and muscle and joint pain, thereby limiting their clinical applications.[6] Therefore, in the treatment of thrombocytopenia, an effective and safe modality that promotes platelet production remains an urgent and unmet medical need.

Thrombopoietin, a glycoprotein predominantly produced by liver cells,[7] is the primary regulator of platelet production by promoting the survival, proliferation, and differentiation of megakaryocytes.[8] The TPO receptor, also known as c-mpl, is expressed on $CD34^+$ cells, megakaryocytes, platelets, and endothelial cells. The receptor changes its conformation upon binding to TPO, subsequently activating a number of signal transduction pathways such as MAPK, PI3 K-AKT, and JAK-STAT that promote the survival, proliferation, and polyploidization of megakaryocytes.[9] It has been reported that administration of TPO to mice significantly increased the number of megakaryocytes in bone marrow and elevated platelet levels by four- to six-fold.[10] Moreover, platelet counts were reduced by approximately 90% in TPO-deficient mice compared to wild-type mice,[11] indicating that TPO plays an important role in regulating megakaryocytopoiesis and thrombopoiesis. Therefore, increasing the production of platelets by upregulating TPO expression may be an important strategy for ameliorating thrombocytopenia.

Photobiomodulation therapy (PBMT) has recently been considered as a therapeutic advancement to induce non-thermo-related biological events such as enhancing cell survival and proliferation,[12,13] accelerating wound healing,[14,15] and regulating neuronal functions.[16,17] Zhang et al. reported that PBMT could protect megakaryocytes from mitochondrial injury and apoptosis, bolster megakaryocytes maturation, and then ameliorate thrombocytopenia.[18,19] However, the mechanisms of PBMT on thrombopoiesis are poorly understood. As a drug-free and noninvasive physical treatment, a growing body of experimental and clinical studies has shown that PBMT could induce a series of complex signaling events, which were triggered by reactive oxygen species (ROS), the main contributing factor of PBMT treatment.[20,21] Currently, the biological mechanism of these effects is still not fully understood by researchers.

In this study, we show, for the first time, that PBMT increases platelet production and ameliorates CIT by upregulating hepatic TPO expression, which is transcriptionally regulated via the activated Src/ERK/STAT3 signaling pathway. Moreover, ROS generation is essential for the activation of Src and its downstream signaling pathways. These findings provide further evidence for PBMT as a novel therapeutic strategy for the control of CIT progression by targeting TPO production.

Essentials

- Photobiomodulation therapy (PBMT) increases platelet production and then ameliorates chemotherapy-induced thrombocytopenia (CIT).
- PBMT upregulates hepatic thrombopoietin (TPO) expression via the activated Src/ERK/STAT3 signaling pathway.
- Reactive oxygen species are responsible for PBMT-induced activation of Src and its downstream target effects.
- PBMT may be a promising avenue for the treatment of CIT.

2 | METHODS

2.1 | Antibodies and reagents

The following reagents were used: H_2DCFDA (10 μM), actinomycin D (Act D, 2 μg/ml), N-acetyl-L-cysteine (NAC, 250 μM), thiazole orange (TO, 0.1 mg/ml), RNase, 4′6-diamidino-2-phenylindole (DAPI), fibrinogen and 5-fluorouracil (5-FU) and were purchased from Sigma-Aldrich. Phalloidin and propidium iodide (PI) were purchased from Beyotime Institute of Biotechnology. PP1 (5 μM), PD98059 (10 μM), and AG490 (50 μM) were purchased from Med Chem Express (MCE). Primary and secondary antibodies, their sources, and the concentrations used are listed in Table S1 in supporting information.

2.2 | Mice

Female C57BL/6 mice (7–8 weeks) were purchased from the Animal Laboratory Center of Southern Medical University. The mice were maintained in a 12-h light/dark cycle. For CIT, mice were treated once by intraperitoneal injection of 5-FU at a dose of 150 mg/kg body weight.[22,23] During the experiment, PBMT was given once daily for three consecutive days starting at 6 h after 5-FU injection. For in vivo ROS-scavenging experiments, mice were treated with NAC (100 mg/kg) 2 days before 5-FU injection. NAC was injected intraperitoneally every day 1 h before PBMT.[24,25]

This study was performed in accordance with the Guide for the Care and Use of Laboratory Animals (Institute of Laboratory Animal Resources, Commission on Life Sciences, National Research Council). All mice studies were approved by the Institutional Animal Care and Use Committee of South China Normal University (Guangzhou, China).

2.3 | Cell culture

The human megakaryoblastic cells (MEG-01) were kindly provided by Dr Wai Ho Tang (Institute of Pediatrics, Guangzhou Women and Children's Medical Center, China) and cultured in RPMI 1640 medium supplemented with 4.5% L-glutamine and 10% FBS (fetal bovine serum). Human hepatocarcinoma HepG2 cells were maintained in Dulbecco's modified Eagle's medium, containing 10% FBS, penicillin (100 U/ml), and streptomycin (100 μg/ml). Cells were incubated at 37°C in a humidified incubator (5% CO_2 and 95% air).

2.4 | PBMT treatment in vivo and in vitro

For the cell experiments, cells were serum-starved overnight and then irradiated with a 635-nm semiconductor laser (NL-FBA-2.0-635, nLight Photonics Corporation) and/or treated with different chemicals. Throughout each of the experiments, the cells were kept either in a complete dark or very dim environment, except when exposed to laser irradiation, to minimize the interference of ambient light. The whole process was conducted at room temperature.

In the animal experiments, to receive the same dose of laser in the liver, the actual power of the laser after penetrating the skin and abdominal cavity into the liver was measured and calculated. The mice were restrained in a specially designed holder after abdominal hair removal and their abdomens were directly irradiated in a vertical irradiation direction from bottom to top with the 635-nm semiconductor laser. The area of laser irradiation to the abdomen of the mice was 2.5 cm × 1 cm, which completely covered the liver of the mice. The rate loss of laser intensity through the mice abdominal wall was approximately 5.823 times.[26] The power density of PBMT was 43.88 mW/cm^2, with a total exposure time of 10 min to obtain an energy density of 23.292 J/cm^2, which corresponds to a dose of 4 J/cm^2 reaching the liver. The control group was maintained in a specially designed stent for the same amount of time as the irradiated group, but the laser source was not activated (sham irradiation).

2.5 | Platelet count

Platelet counts were determined by an automatic blood cell analyzer (HF-3800, Kang Yu Medical). About 10–30 μl of peripheral blood from mice were collected into ethylenediaminetetraacetic acid (EDTA)-coated tubes and immediately mixed. In this part, whole blood was used without any dilution, and results were excluded in cases in which there was clotting in the sample.

2.6 | MEG-01 ploidy analysis

MEG-01 cells were collected, washed thrice with phosphate-buffered saline (PBS), and centrifuged for 5 min at 100 *g* at 4°C. The pellets were resuspended in 75% ethanol overnight at 4°C. Afterward, the cells were washed with PBS and centrifuged at 100 *g* for 5 min at 4°C. The pellets were resuspended in PBS and treated with RNase (5 μg/ml, 30 min, 37°C) and then stained with PI (10 μg/ml, 30 min, 4°C). Samples were examined with a BD FACSCanto II flow cytometer (Becton Dickinson) and analyzed using FCS Express software (De Novo Software).

2.7 | Platelet production assay

Platelet production (reticulated platelets [RPs]) was measured by flow cytometry as previously described.[27] Briefly, a small amount of whole blood was collected from the tail vein and placed in anticoagulant. Whole blood (10 μl) was incubated with 3 μl APC-CD61 and 90 μl of PBS for 30 min in the dark at room temperature. After incubation, 500 μl TO (0.1 mg/ml) was added and incubated again for 30 min under the same conditions. Platelets were recognized by analyzing size (forward scatter), granularity (side scatter), and specific membrane antigens (CD61). We used platelet population as a gate to detect RPs using flow cytometry and TO-positive platelets were considered reticulated.

2.8 | Platelet-like particle analysis

MEG-01-derived platelet-like particles (PLPs) were isolated by sequential centrifugation (150 *g*, 10 min; 500 *g* 10 min; 1000 *g* 10 min) of MEG-01 cell supernatants under different treatment conditions. PLPs were identified by their size, granulation, and capacity to bind anti-CD41 using normal human platelets from peripheral blood as control.[28,29] For human blood platelet isolation, whole blood was obtained from donors and with South China Normal University Institutional Review Board approval (SCNU-BIP-2020-003). Platelets were obtained by centrifugation as previously described.[30] Informed consent was obtained from all donors in accordance with the Declaration of Helsinki. MEG-01-derived PLPs and peripheral blood platelets were stained with fluorescein isothiocyanate (FITC)-CD41 antibody and detected by flow cytometry.

2.9 | Analysis of proplatelet formation

To analyze proplatelet formation (PPF), first, MEG-01 cells from different treatment groups were harvested and plated onto fibrinogen-coated coverslips in 12-well plates. Then, the cells were fixed in 4% paraformaldehyde, permeabilized with 0.2% Triton X-100, blocked with 5% bovine serum albumin (BSA), and stained with β-tubulin antibody, phalloidin, and DAPI. MEG-01 cells extending proplatelets were identified as cells extending long filamentous structures ending with platelet-sized tips.[31,32] Images were captured using confocal microscopy (LSM880 META; Carl Zeiss MicroImaging), and the number of MEG-01 cells producing proplatelets was determined using Zeiss Zen Blue Edition Software (Carl Zeiss MicroImaging).

2.10 | Tail bleeding time

Non-anesthetized mice were placed in a restraining device, and tails were transected at 5 mm from the tip. The tails were immersed in pre-warmed PBS at 37°C, and the time from severing to cessation of bleeding was recorded as bleeding time. If bleeding did not cease, then observation would be stopped at 120 s.

2.11 | Western blot analysis

Western blotting was performed following our previous description with some modifications.[33] Briefly, cells were lysed in cold lysis buffer, protein samples (60 μg) were separated by sodium dodecyl sulfate polyacrylamide gel electrophoresis (SDS-PAGE), and transferred to a polyvinylidene difluoride membrane (Millipore). The membranes were washed with Tris-buffered saline with 0.1% Tween-20 (TBST) thrice, blocked with 5% skim milk, and then incubated with the primary antibodies overnight at 4°C. Afterward, the membranes were washed with TBST thrice and incubated with fluorescent secondary antibody for 2 h at room temperature. Detection was performed using the Odyssey Infrared Imaging System (LI-COR, Biosciences). The intensity of the western blot signals was quantified using ImageJ software (National Institutes of Health). The results of densitometry analyses are presented as the ratio of protein/β-tubulin protein; and are compared to controls and normalized to 1.

2.12 | Flow cytometry analysis

The femur and tibia were collected from mice, and marrow was flushed out with PBS. A single-cell suspension was prepared through individual 74 μm cell strainer and washed thrice in PBS. Cells were lysed in ammonium-chloride-potassium (ACK) lysis buffer to remove red blood cells and then centrifuged for 5 min at 800 *g* at 4°C. The pellets were resuspended in 100 μl of PBS containing FITC-CD41 and PE-CD61 antibodies. Cells were stained at room temperature for 30 min in the dark. The number of megakaryocytes in bone marrow was determined by gating for both CD41/61 positivity, and the cell population was analyzed by flow cytometry.

Bone marrow cells of mice in different treatment groups were incubated with FITC-CD41 antibody for 30 min at room temperature, then treated with RNase and PI. The DNA content of $CD41^+$ megakaryocytes was quantified by flow cytometry and analyzed using FCS Express software.

2.13 | Immunofluorescence

After treatment under different experimental conditions, the cells were fixed in 4% paraformaldehyde for 15 min, followed by permeabilization in 0.2% Triton X-100 for 30 min. The cells were incubated with 5% BSA for 1 h at 37°C to block unspecific binding and incubated overnight at 4°C with primary antibodies. The cells were washed with PBS and then incubated with fluorescent secondary antibodies for 2 h. After three additional washes with PBS, the slides were mounted and analyzed by confocal microscopy.

2.14 | mRNA extraction and quantitative real-time polymerase chain reaction

The total RNA was isolated from the liver of mice or HepG2 cells using RNAiso Plus (TaKaRa, D9108A). Primers (Table S2 in supporting information) were designed and synthesized by Invitrogen. The ReverTra Ace quantitative polymerase chain reaction (qPCR) RT Master Mix with gDNA Remover (Toyobo, FSQ-301) was used to synthesize cDNA. Quantitative real-time PCR was performed using the SYBR-Green qPCR Super Mixture (Takara, RR820A) on a Real-Time Detection System (BioRad). The amount of cDNA was normalized to the intensity of the PCR products of GAPDH. All the amplified products were observed using the Quantity One software (Bio-Rad). qPCR was performed in triplicate.

2.15 | Bone marrow histology

Mice femurs were fixed in 4% paraformaldehyde, decalcified, and dehydrated. Tissues were embedded in paraffin, sectioned, and stained with hematoxylin and eosin (H&E). The morphology of the bone marrow was assessed by light microscopy (Leica DMLB, Leica). Megakaryocytes were counted throughout the whole slice of the samples.

2.16 | SiRNA-mediated gene silencing

For siRNA-mediated gene silencing, we used STAT3-specific siRNA (Table S3 in supporting information).[34] All siRNAs were synthesized by GenePharma. Cells were transfected specific siRNA oligonucleotides using Lipofectamine 3000. HepG2 cells were harvested 48 h after transfection and subjected to western blot analysis using anti-TPO antibody.

2.17 | Imaging analysis of living cells

To visualize living cells, HepG2 cells were transfected with STAT3-yellow fluorescent protein (YFP). After 48 h expression, the nuclei were stained with DAPI. Using confocal microscopy, we imaged the distribution pattern of STAT3-YFP and DAPI simultaneously after PBMT. Cells were also maintained at 37°C and 5% CO_2 during imaging within the culture chamber.

2.18 | Measurement of TPO levels

Plasma TPO levels of mice and supernatant TPO levels of HepG2 cells were measured using the Mice Thrombopoietin Quantiken ELISA kit and Human Thrombopoietin Quantiken ELISA kit (Wuhan

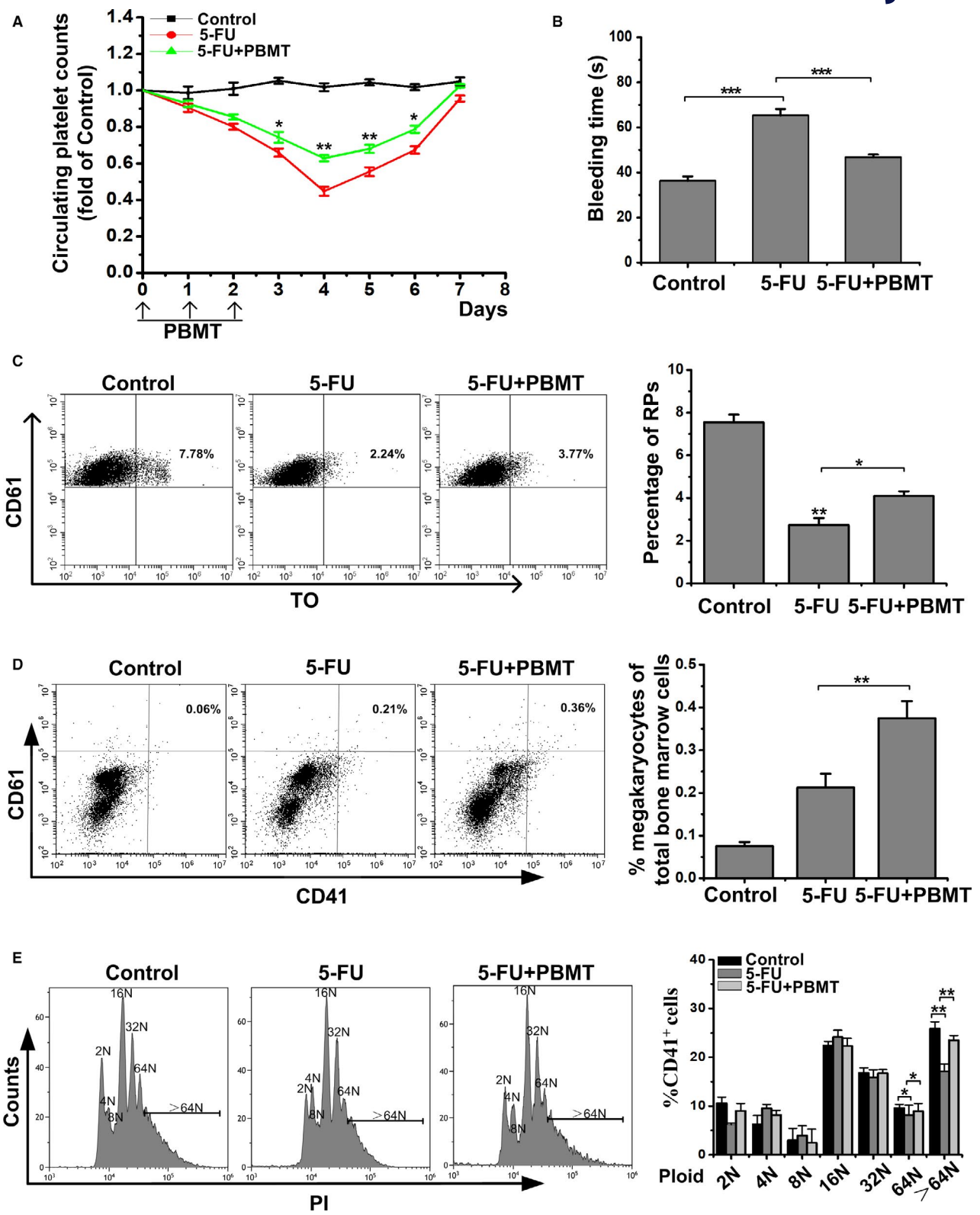

FIGURE 1 Photobiomodulation therapy (PBMT) alleviates 5-fluorouracil (5-FU)-induced thrombocytopenia in mice. A, Platelet counts were measured daily at 4 h after PBMT by automatic blood cell analyzer. B, Tail bleeding time was examined on day 4. C, Percentage of reticulated platelets was determined as CD61/TO-positive signals by flow cytometry on day 3. D, The number of megakaryocytes in bone marrow from femur and tibia was measured by flow cytometry. E, Ploidy analysis of $CD41^+$ megakaryocytes in bone marrow from femur and tibia. Cells were stained with fluorescein isothiocyanate (FITC)-CD41 antibody and propidium iodide, followed by flow cytometric analysis of DNA content. Data are presented as mean ± standard error of the mean. n = 8 animals per group. $^*P < .05$; $^{**}P < .01$, $^{***}P < .001$

Colorful-Gene Biological Technology) respectively, which were both in accordance with the manufacturer's instructions.

2.19 | Intracellular ROS assay

Laser scanning confocal microscopy was used to assess intracellular ROS generation.[35] HepG2 cells were cultured in confocal dishes with corresponding treatment. When cells reached 70% to 80% confluency, these were washed with PBS and loaded with 10 μM H_2DCFDA for 30 min at 37°C. Finally, the cells were washed with PBS and imaged using an LSM 510 confocal microscope (Carl Zeiss).

Intracellular ROS levels were also measured by flow cytometry.[36] Cells were washed thrice with PBS and incubated with H_2DCFDA for 30 min at 37°C. Subsequently, cells were washed with PBS, trypsinized, and resuspended in PBS solution. Total intracellular fluorescence intensity was measured for 10,000 cells from each sample by flow cytometry.

2.20 | Statistical analysis

All assays were repeated independently at least thrice. Statistical analyses were performed using one-way analysis of variance to compare more than two groups or Student's *t*-test to compare two groups of independent samples. All quantitative data were presented as mean ± standard error of the mean (SEM). Differences with $p < .05$ were deemed statistically significant.

3 | RESULTS

3.1 | PBMT alleviates 5-FU--induced thrombocytopenia in mice

As a remedy commonly used in oncology, 5-FU exhibits high toxicity that can result in severe myelosuppression and thrombocytopenia.[37] To investigate the thrombopoietic effects of PBMT, a mouse model of CIT was created by injecting 5-FU once at a dose of 150 mg/kg body weight. The mice were treated with 4 J/cm^2 PBMT after 5-FU injection 6 h, and PBMT treatment was continued for 2 days. The level of circulating platelets in mice markedly decreased after administration of 5-FU (Figure 1A). PBMT accelerated the recovery in platelet count in the presence of 5-FU. Moreover, bleeding time was approximately two-fold longer in mice on day 4 after 5-FU injection, but PBMT could significantly shorten tail bleeding time in thrombocytopenic mice (Figure 1B). To further determine whether platelet production increased in PBMT-treated thrombocytopenic mice, the number of RPs was measured using TO staining.[38,39] The percentage of RPs was approximately 1.5-fold higher in the blood of PBMT-treated thrombocytopenic mice than in non-treated thrombocytopenic mice (Figure 1C). These results showed that PBMT increased the production of platelets in 5-FU--induced thrombocytopenic mice.

Platelets are produced from megakaryocytes residing in bone marrow. Thus, we investigated the number and ploidy of megakaryocytes in bone marrow. We used a semiconductor laser to directly irradiate the abdomen of thrombocytopenic mice, and the number of megakaryocytes in bone marrow from femur and tibia was determined by flow cytometry. As expected, the number of megakaryocytes in the bone marrow of thrombocytopenic mice significantly increased after PBMT treatment (Figure 1D). Additionally, H&E staining of mouse bone marrow paraffin sections revealed the same results (Figure S1 in supporting information), which further supported the above conclusion. Then, we examined whether PBMT could promote bone marrow megakaryocyte maturation in thrombocytopenic mice, and the results showed that the proportion of ≥64 N megakaryocytes in bone marrow increased in the PBMT-treated group compared to the non-treated thrombocytopenic mice group (Figure 1E), suggesting that PBMT significantly promoted polyploidization of megakaryocytes in the bone marrow of thrombocytopenic mice, thus boosting platelet production. Overall, these findings confirmed that PBMT effectively promoted megakaryocytopoiesis and thrombopoiesis.

3.2 | PBMT upregulates TPO expression both *in vivo* and *in vitro*

Previous studies have shown that TPO could support the survival and development of megakaryocyte progenitor cells, induce megakaryocyte maturation, and promote platelet production both *in*

FIGURE 2 Photobiomodulation therapy (PBMT) upregulates thrombopoietin (TPO) expression *in vivo* and *in vitro*. A–C, Mice were injected with 5-fluorouracil (5-FU; 150 mg/kg) on day 0. PBMT was given daily for three consecutive days starting at 6 h after 5-FU injection. Control mice received saline only ($n = 6$). Hepatic thrombopoietin (TPO) expression and secretion were detected by western blot (A) and ELISA (B) in thrombocytopenic mice with or without PBMT. Representative immunofluorescence images of TPO (red) in the livers of different groups of mice (C). 4′6-diamidino-2-phenylindole (DAPI) staining was used to visualize nuclei. Scale bar: 100 μm. D–E, Representative western blot assays to investigate the time- (D) and dose-dependent effects (E) of PBMT on TPO expression in HepG2 cells. F, TPO expression in HepG2 cells after PBMT treatment was assessed by ELISA. G–I, HepG2 cells with or without PBMT were co-cultured with MEG-01 cells for 4 d. G, The ploidy of MEG-01 cells was determined by staining with propidium iodide, followed by flow cytometric analysis of DNA content. H, MEG-01 cells in different treatment groups were cultured on fibrinogen-coated glass slides for 18 h and stained with β-tubulin (green), F-actin (phalloidin, red), and DAPI (blue). Scale bar: 50 μm. I, The number of platelet-like particles (CD41$^+$) produced by MEG-01 cells was determined by flow cytometry. Data are presented as mean ± standard error of the mean. $^*P < .05$; $^{**}P < .01$

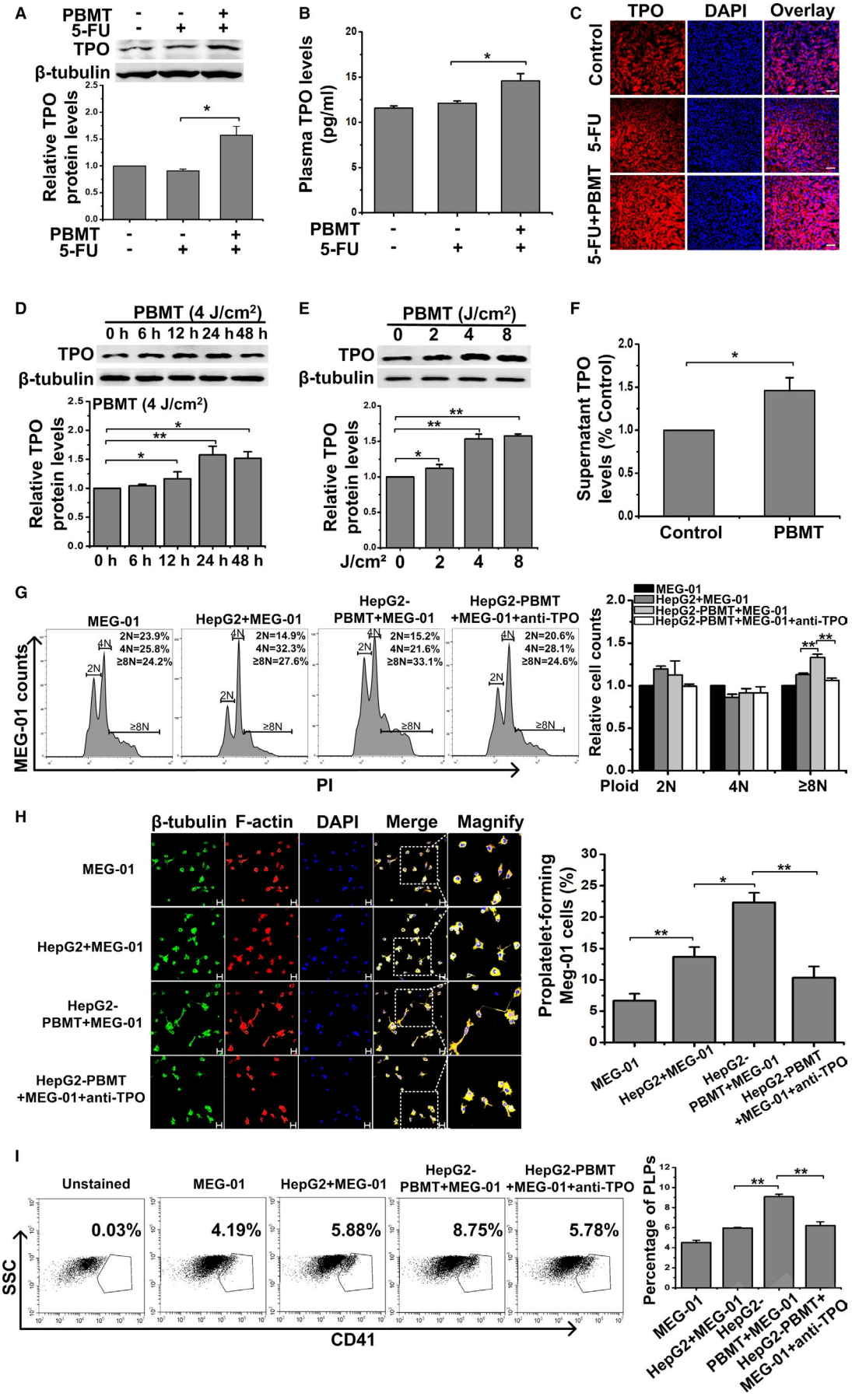

vivo[40] and *in vitro*.[41] TPO is mainly secreted by hepatocytes into the blood. To clarify the effects of PBMT on TPO expression *in vivo*, we first assessed the mRNA and protein expression levels of hepatic TPO in mice from different treatment groups. qPCR and western blot analysis of the liver homogenate samples demonstrated that hepatic TPO mRNA (Figure S2A in supporting information) and protein expression levels (Figure 2A) in thrombocytopenic mice significantly increased after PBMT treatment. Additionally, plasma TPO levels dramatically increased in thrombocytopenic mice after treatment with PBMT (Figure 2B), and similar results were obtained by immunofluorescence staining (Figure 2C). These results indicated that PBMT upregulated hepatic TPO expression *in vivo*, which increased the level of TPO in the blood.

In vitro, we further examined the expression of TPO in HepG2 cells, and the results showed that the TPO mRNA (Figure S2B) and protein levels (Figure 2D,E) also significantly increased after 4 J/cm^2 PBMT treatment. Moreover, the upregulation of TPO expression and secretion in HepG2 cells caused by PBMT was further demonstrated by immunofluorescence (Figure S2C), flow cytometry (Figure S2D), and ELISA (Figure 2F). These results strongly indicated that PBMT could upregulate TPO expression and secretion *in vitro*.

To further investigate the effects of PBMT-induced upregulation of TPO on megakaryocytes, HepG2 cells with or without PBMT were co-cultured with MEG-01 cells for 4 days. Our results indicated that ploidy (Figure 2G), PPF (Figure 2H), and PLP (Figure 2I) production in MEG-01 cells significantly increased after co-culturing with PBMT-treated HepG2 cells. However, their increase was almost entirely inhibited after treatment with TPO-neutralizing antibody. These results suggested that upregulation of TPO by PBMT induced polyploidization, PPF, and platelet production in MEG-01 cells.

3.3 | Activating STAT3 is responsible for PBMT-induced upregulation of TPO

Next, we investigated whether PBMT-upregulated TPO expression was due to new mRNA synthesis. Act D, as a pharmacological inhibitor of transcription, was employed. We found that mRNA expression of TPO increased in HepG2 cells after PBMT treatment, but the increase of TPO mRNA levels was significantly inhibited after preincubation with Act D (Figure 3A), suggesting that TPO transcription contributed to the increase in TPO protein level that was induced by PBMT.

STAT3 has been reported to participate in the expression of TPO, ultimately promoting platelet production.[42,43] Thus, we examined whether PBMT could activate STAT3 to regulate TPO expression in HepG2 cells. First, we monitored changes in STAT3 in the subcellular localization under PBMT. HepG2 cells were transfected with STAT3-YFP. After 48 h expression, the nuclei were stained with DAPI and the dynamics of STAT3-YFP in positive transfected cells were assessed by confocal microscopy. The results showed that PBMT caused a 1.8-fold increase in STAT3 nuclear fluorescence intensities within 150 min, compared to the control cells (Figure 3B and Figure S3A in supporting information), thereby revealing PBMT-induced nuclear translocation of STAT3. This result was further confirmed in HepG2 cells by immunofluorescence using p-STAT3 antibody (Figure 3C). Meanwhile, we determined the extent of p-STAT3 staining in HepG2 cells by flow cytometry and the results showed that the fluorescence intensity of p-STAT3 significantly increased after PBMT treatment (Figure S3B). The phosphorylation level of STAT3 in the nucleus also increased after PBMT (Figure 3D). These findings showed that PBMT activated STAT3 and promoted STAT3 translocation to the nucleus.

To further investigate whether PBMT-induced STAT3 activation regulates TPO expression, HepG2 cells were pretreated with Stattic (a specific inhibitor of STAT3) before PBMT treatment. The result showed that pretreatment of HepG2 cells with Stattic significantly inhibited the increases induced by PBMT in STAT3 phosphorylation and TPO expression (Figure 3E). Furthermore, HepG2 cells were transfected with STAT3 siRNA, which revealed that knocking down STAT3 antagonized the PBMT-induced upregulation of TPO (Figure 3F). All these results suggested that activating STAT3 is responsible for PBMT-induced upregulation of TPO.

3.4 | PBMT activates STAT3 via the Src/ERK pathway

To identify the kinases activated by PBMT that are responsible for STAT3 activation in HepG2 cells, we studied the effect of specific inhibitors of these signaling pathways: PD98059, PP1, and AG490 (for MEK/ERKs, Src, and JAK, respectively) using western blot assays. The results showed that PBMT increased the phosphorylation level of STAT3 in HepG2 cells, which was reversed by pretreatment with PD98059 and PP1, but not AG490 (Figure 4A).

To further confirm that ERK and Src were involved in PBMT-induced STAT3 activation, western blot assays were performed to examine the effects of ERK and Src activation on STAT3 phosphorylation in response to PBMT in HepG2 cells. The protein levels of p-Src, p-ERK, p-STAT3, and TPO significantly increased in HepG2 cells after PBMT treatment (Figure 4B,C). However, preincubation of

FIGURE 3 Activated STAT3 is responsible for photobiomodulation therapy (PBMT)-induced upregulation of thrombopoietin (TPO). A, TPO mRNA levels in HepG2 cells stimulated by PBMT in the presence of Act D (2 μg/ml) were assessed by quantitative polymerase chain reaction. B, Representative time-series images of HepG2 cells expressing STAT3-YFP with or without PBMT treatment. Staining with 4′6-diamidino-2-phenylindole (DAPI) to visualize nuclei. Scale bar: 5 μm. C, Representative immunofluorescence images of p-STAT3 in HepG2 cells. Staining with DAPI to visualize nuclei. Scale bar: 10 μm. D, Representative western blot assay to investigate the phosphorylation levels of STAT3 in nuclear (Nuc) and cytoplasm (Cyto) lysates of HepG2 cells after PBMT. E–F, Western blot analysis of TPO expression in PBMT-treated HepG2 cells after treatment with Stattic (5 μM) (E) and STAT3 siRNA (F). Data are presented as mean ± standard error of the mean. *P < .05; **P < .01

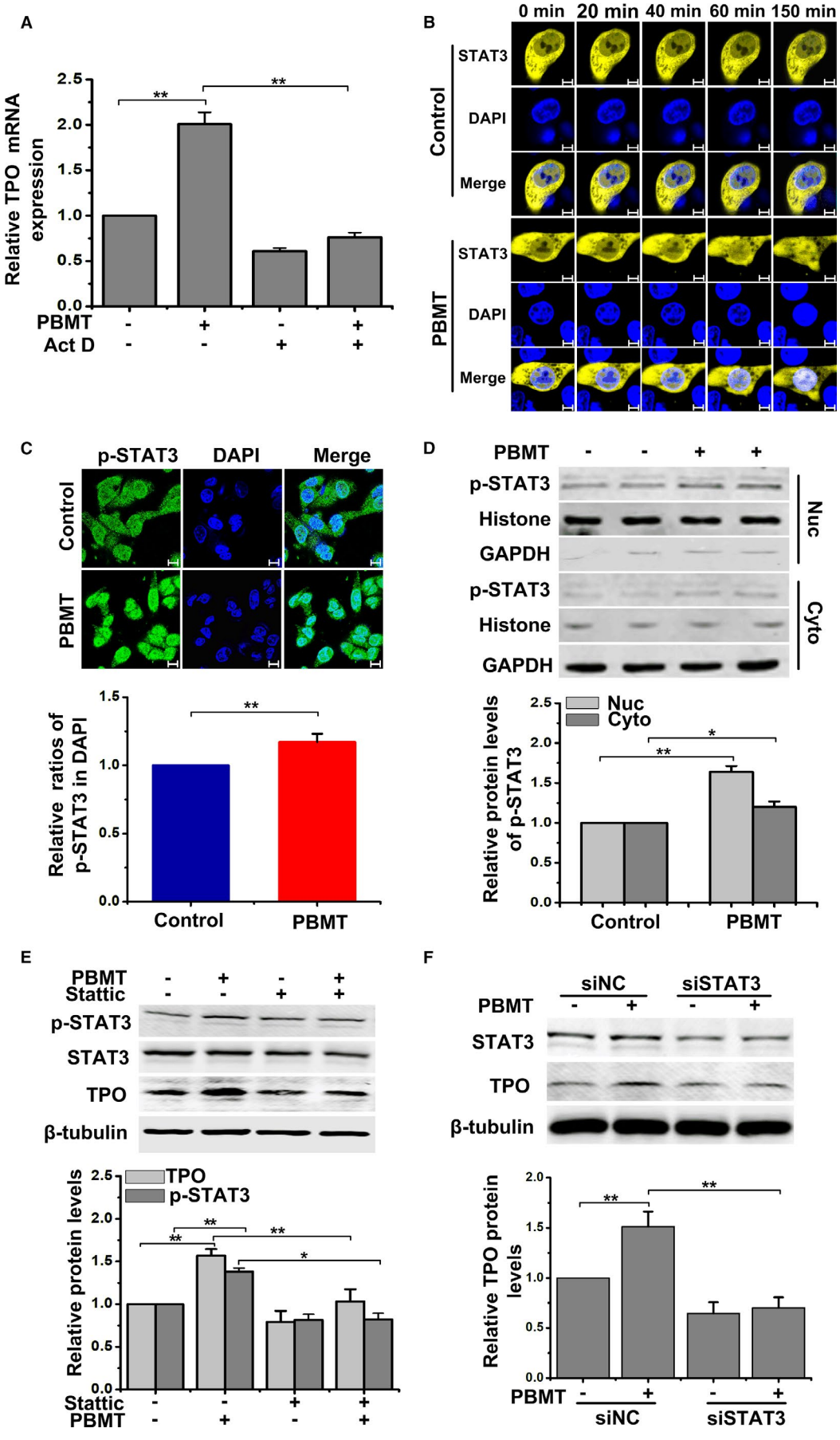

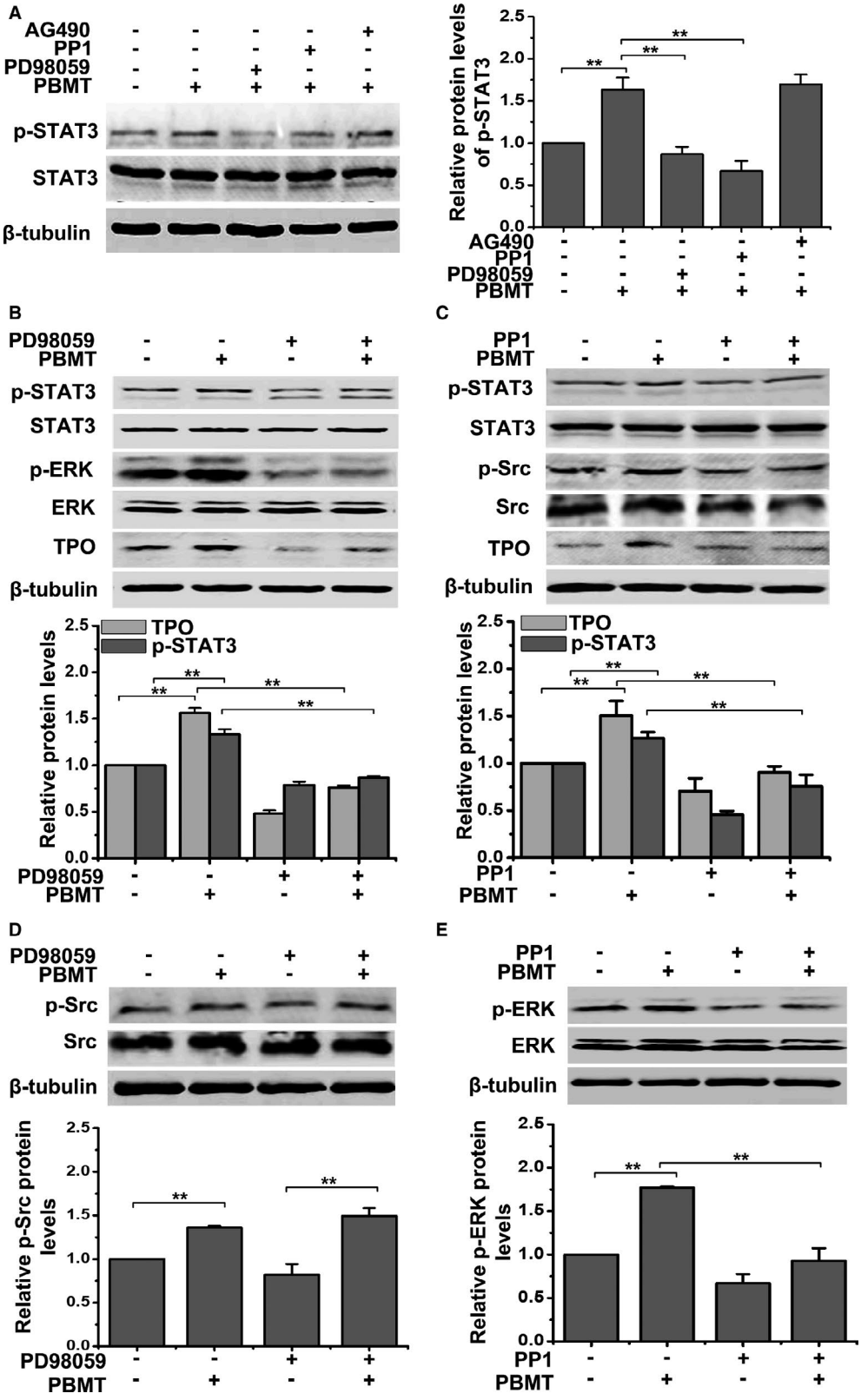

FIGURE 4 Photobiomodulation therapy (PBMT) activates STAT3 via the Src/ERK pathway. A, Representative western blot assay of STAT3 phosphorylation in HepG2 cells after treatment with PBMT in the presence of PP1 (5 μM), PD98059 (10 μM), and AG490 (50 μM). B–C, Western blot analysis was performed to detect the levels of p-STAT3 and thrombopoietin after treatment with PBMT in the presence of PD98059 (B) and PP1 (C). D, Representative western blot assay for detecting the levels of p-Src in PBMT-treated HepG2 cells after treatment with PD98059. E, Representative western blot assay for detecting the levels of p-ERK in HepG2 cells after treatment with PBMT in the presence of PP1. Data are presented as mean ± standard error of the mean. $^{**}P < .01$

PD98059 and PP1 to inhibit ERK and Src, respectively, both resulted in a decrease in STAT3 phosphorylation and TPO expression, suggesting that ERK and Src are involved in PBMT-induced upregulation of TPO expression. Western blot assays were further performed to investigate the relationship between ERK and Src in HepG2 cells after PBMT treatment. We found that when HepG2 cells were pre-incubated with PD98059, the phosphorylation level of Src did not change after PBMT treatment (Figure 4D). However, inhibition of Src by treatment with PP1 before PBMT resulted in decreased phosphorylation levels of ERK (Figure 4E), indicating that Src is located upstream of ERK in PBMT-treated HepG2 cells. These results show that PBMT activates the Src/ERK/STAT3 pathway to upregulate TPO expression.

3.5 | PBMT-induced Src/ERK activation is dependent on the generation of ROS

It has been suggested that the production of ROS is responsible for the biostimulative effect of PBMT.[44] Thus, we explored whether PBMT increased the generation of ROS in HepG2 cells. HepG2 cells were monitored by measuring changes in fluorescence caused by oxidation of intracellular H_2DCFDA (nonfluorescent) to DCF (fluorescent), whose fluorescence intensity indicates the relative level of ROS production. We found that the level of intracellular ROS apparently increased in HepG2 cells after PBMT treatment, but ROS scavenger NAC inhibited the PBMT-induced increase in ROS (Figure 5A). These results were further confirmed by flow cytometry analysis (Figure 5B). To further investigate whether ROS are indispensable for Src activation, we pretreated HepG2 cells for 1 h with NAC before PBMT. The results showed that administration of NAC inhibited Src, ERK, and STAT3 activation and prevented the increase in TPO protein levels in PBMT-treated HepG2 cells (Figure 5C). These results were also confirmed by immunofluorescence staining with p-STAT3 and TPO antibodies in HepG2 cells (Figure 5D and Figure S4A,B in supporting information).

To directly demonstrate that PBMT induced an increase in TPO expression via an ROS-dependent signaling pathway *in vivo*, we administrated NAC to mice 2 days before 5-FU injection. We found that the phosphorylation levels of ERK, Src, and STAT3 and the expression of TPO significantly increased in thrombocytopenic mice after PBMT treatment, but administration of NAC inhibited these PBMT-induced effects (Figure 5E). Furthermore, plasma TPO contents and hepatic TPO mRNA levels dramatically decreased after NAC application to PBMT-treated thrombocytopenic mice (Figure 5F and Figure S4C), and similar results were obtained by immunofluorescence staining (Figure S4D). We also found that the increase in the number of RPs in PBMT-treated thrombocytopenic mice decreased after treatment with NAC (Figure 5G). Together, these findings show that the ROS-dependent Src/ERK/STAT3 signaling pathway induced by PBMT triggers TPO expression, thereby increasing platelet production.

4 | DISCUSSION

To the best of our knowledge, this is the first time that PBMT has been found to promote thrombopoiesis through upregulating TPO expression. We demonstrated that the beneficial effects of PBMT are correlated with its ability to induce intracellular ROS generation and activate the Src/ERK/STAT3 signaling pathway, leading to upregulated TPO expression and enhanced platelet production. Therefore, understanding the mechanism and functional significance of PBMT may provide a safe and effective therapeutic strategy for CIT.

PBMT is a non-thermal form of irradiation using light in the visible to near-infrared range and has been used clinically to promote hair growth[45] and reduce pain and inflammation in various pathologies.[46] Moreover, recent reports have suggested that PBMT could promote the maturation of megakaryocytes and increase platelet production.[18,19] This raised our interest to explore the potential protective mechanisms of PBMT in patients with thrombocytopenia.

As expected, we found that PBMT significantly increased peripheral platelet counts and reduced tail bleeding time in thrombocytopenic mice. All platelet counts in mice returned to their normal range on day 7; the increase was regarded as a compensatory response to the decrease in platelet count. Moreover, the number and ploidy of bone marrow megakaryocytes significantly increased in PBMT-treated thrombocytopenic mice. Therefore, PBMT may have high clinical relevance. What is the reason for the increase in the number and ploidy of megakaryocytes after PBMT treatment? Some reports have shown that TPO promotes the differentiation and maturation of megakaryocytes.[47,48] Based on these findings, we hypothesized that PBMT upregulates the expression of TPO, which in turn promotes megakaryocytopoiesis and increases platelet production. Our results supported this hypothesis in that the expression of TPO significantly increased *in vivo* and *in vitro* after PBMT treatment. Further *in vitro* studies demonstrated that upregulation of TPO by PBMT induced polyploidization, PPF, and platelet production in MEG-01 cells. However, the increase in MEG-01 cell ploidy, PPF, and PLPs counts was significantly inhibited by anti-TPO neutralizing antibodies. These results indicate that PBMT promotes platelet production by upregulating hepatic TPO expression, thereby ameliorating thrombocytopenia.

Previous research has shown that STAT3 is involved in regulating TPO synthesis, thereby regulating platelet production.[42] To investigate whether PBMT could activate STAT3 and the relationship between STAT3 and TPO in HepG2 cells under PBMT treatment, we first examined the effect of PBMT on STAT3 by live cell imaging, immunofluorescence, and western blot assays. As expected, we confirmed that PBMT promoted the translocation of STAT3 to the nucleus. These findings suggest that the effects of PBMT on TPO may be attributable to STAT3 phosphorylation. Our results supported this hypothesis because both pharmacological inhibition and knockdown of STAT3 could block PBMT-mediated upregulation of TPO expression.

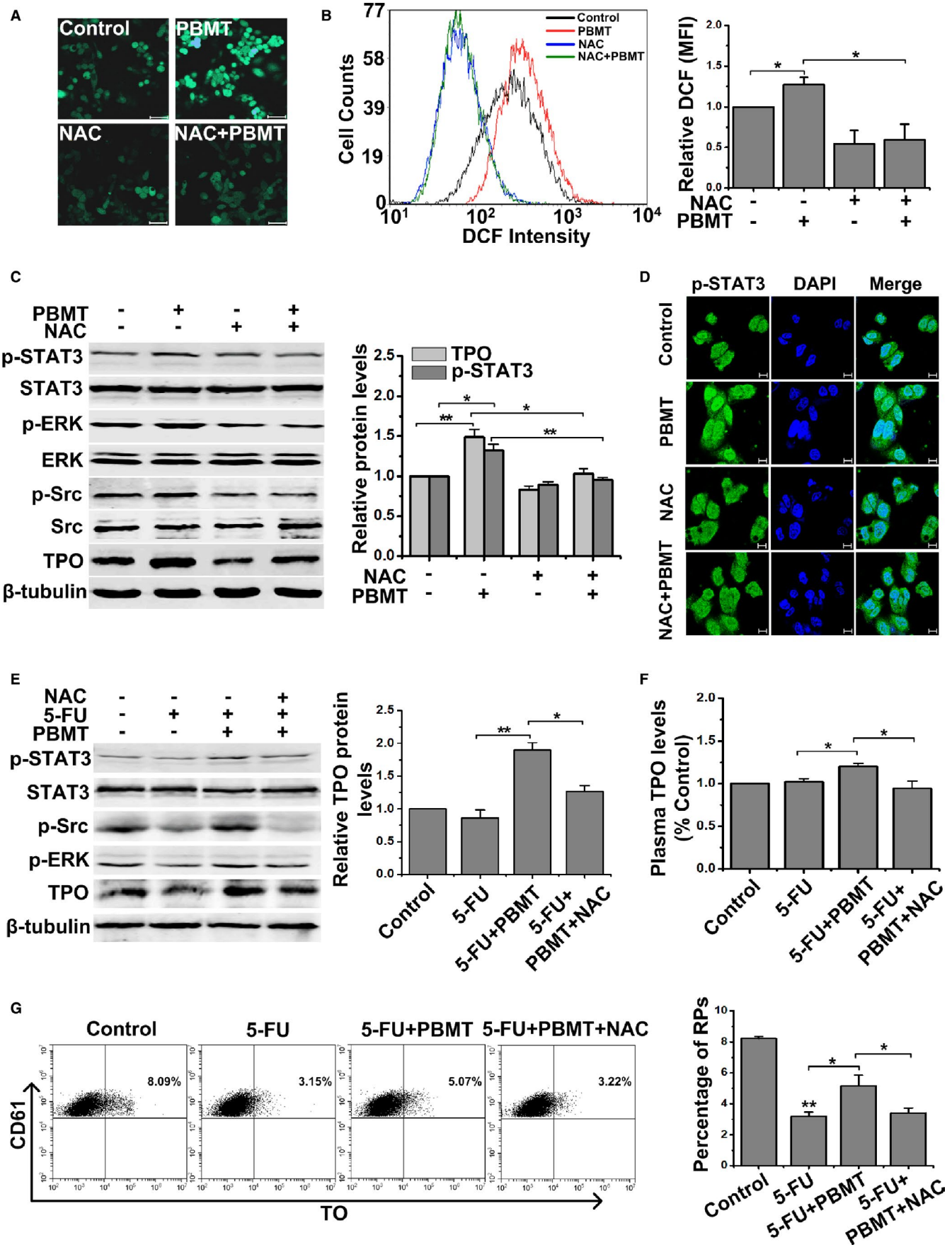

FIGURE 5 Photobiomodulation therapy (PBMT)-induced Src/ERK activation is dependent on the generation of ROS. A–B, ROS generation in H2DCFDA labeling HepG2 cells with indicated treatments was assessed by confocal microscopy (A) and flow cytometry (B). C, Western bolt analysis of p-Src, p-ERK, p-STAT3, and thrombopoietin (TPO) levels in PBMT-treated HepG2 cells after treatment with N-acetyl-L-cysteine (NAC). D, Representative immunofluorescent images of p-STAT3 in HepG2 cells under the indicated treatments. Staining with 4′6-diamidino-2-phenylindole to visualize nuclei. Scale bar: 10 μm. E–G, Mice were treated daily with 100 mg/kg NAC 2 days before 5-fluorouracil (5-FU) injection ($n = 6$). After 5-FU injection, PBMT was given daily for three consecutive days. E, Western blot analysis of total liver lysates in mice of different treatment groups on day 3. F, Hepatic TPO secretion of mice in different treatment groups was detected by ELISA. G, Percentage of reticulated platelets was determined as CD61/TO-positive signals on day 3 in different mouse treatment groups by flow cytometry. Data are presented as mean ± standard error of the mean. $^{*}P < .05$; $^{**}P < .01$

Although STAT3 can be activated by ERK, Src, and JAK,[42,49,50] the present study found that inhibition of ERK and Src activity suppressed PBMT-induced STAT3 phosphorylation in HepG2 cells. We also found the activation of ERK in HepG2 cells caused by PBMT was prevented after treatment with PP1. The results indicated that PBMT-induced nuclear translocation of STAT3 is mediated by the Src/ERK pathway. How could Src activate the ERK signaling pathway? It has been reported that activated c-Src can phosphorylate Shc on tyrosines to provide docking sites for downstream signaling proteins.[51] In particular, tyrosine-phosphorylated Shc can recruit Grb2/SOS through association between the Grb2 SH2 domain and Shc phosphotyrosine residues,[52] thereby resulting in the activation of the ERK pathway.

How could PBMT activate the Src/ERK/STAT3 signaling pathway? Previous reports have indicated that PBMT causes an increase in intracellular ROS levels, which in turn activates Src. The activation of Src by ROS can be explained by the ability of ROS to oxidize thiol groups or inactivate protein tyrosine phosphatases (PTPs) of Src.[53,54] ROS can upregulate intracellular protein tyrosine phosphorylation through the specific oxidation of cysteine SH groups on protein tyrosine kinases in Src, resulting in a conformational change that is necessary for Src activation.[55] In addition to direct oxidation, ROS can also mediate the inactivation of PTPases, thereby changing the equilibrium and resulting in the activation of downstream signaling pathways.[56]

What is the mechanism of ROS generation caused by PBMT? It has been widely reported that after PBMT treatment, light is absorbed by endogenous chromophores (porphyrins or cytochromes) that are predominantly located in the plasma membrane, lysosomes, or mitochondria, and the excitation of intracellular chromophores leads to the generation of ROS.[54,57,58] ROSs act as common secondary messengers that play important roles in light signal transduction pathways.[59] We confirmed that PBMT could increase intracellular ROS levels in HepG2 cells and pretreatment with NAC significantly attenuated the activation of Src, ERK, and STAT3, indicating that PBMT-induced activation of Src, ERK, and STAT3 is ROS-dependent.

Overall, the current investigation demonstrated that PBMT upregulates the expression of TPO via a ROS-dependent Src/ERK/STAT3 pathway in hepatic cells, thereby increasing platelet production and ameliorating CIT. Importantly, the upregulation of TPO expression by PBMT is likely an important step for ameliorating CIT. PBMT may be a promising avenue for the treatment of CIT, and elucidating the regulatory mechanism of photobiomodulation may provide a therapeutic strategy for controlling the progression of thrombocytopenia. It is worth noting that this modality is not intended to replace platelet transfusion to control bleeding, but rather to greatly reduce the need for platelet transfusion and prevent thrombocytopenia.

ACKNOWLEDGMENTS

This work was supported by the National Natural Science Foundation of China (Nos. 62005085, 61361160414 and 31470072), the Science and Technology Program of Guangzhou (No. 2019050001), the Science and Technology Project of Guangzhou (No. 201805010002), and the Science and Technology Planning Project of Guangdong Province (Guangdong-Hong Kong Joint Innovation Project), China (No. 2014B050504009).

CONFLICTS OF INTEREST

The authors declare no competing financial interests.

AUTHOR CONTRIBUTIONS

Q. H. Wang, H. C. Chang, and D. Xing designed the research. Q. H. Wang, Y. H. Li, and H. C. Chang performed the experiments. Q. H. Wang, H. C. Chang, and Q. Shen analyzed the data. Q. H. Wang, H. C. Chang, and D. Xing drafted and revised the manuscript.

ORCID

Da Xing https://orcid.org/0000-0001-9752-8458

REFERENCES

1. Wu Y, Aravind S, Ranganathan G, Martin A, Nalysnyk L. Anemia and thrombocytopenia in patients undergoing chemotherapy for solid tumors: a descriptive study of a large outpatient oncology practice database, 2000–2007. *Clin Ther*. 2009;31:2416-2432.
2. Lee HR, Yoo N, Jeong J, Sohn KY, Yoon SY, Kim JW. PLAG alleviates chemotherapy-induced thrombocytopenia via promotion of megakaryocyte/erythrocyte progenitor differentiation in mice. *Thromb Res*. 2018;161:84-90.
3. Ding S, Wang M, Fang S, et al. D-dencichine regulates thrombopoiesis by promoting megakaryocyte adhesion, migration and proplatelet formation. *Front Pharmacol*. 2018;9:297.
4. Webert KE, Arnold DM, Lui Y, Carruthers J, Arnold E, Heddle NM. A new tool to assess bleeding severity in patients with chemotherapy-induced thrombocytopenia. *Transfusion*. 2012;52:2466-2474.
5. Hallam S, Provan D, Newland AC. Immune thrombocytopenia-what are the new treatment options? *Expert Opin Biol Ther*. 2013;13:1173-1185.
6. Zeuner A, Signore M, Martinetti D, Bartucci M, Peschle C, Maria RD. Chemotherapy-induced thrombocytopenia derives from the

selective death of megakaryocyte progenitors and can be rescued by stem cell factor. *Cancer Res*. 2007;67:4767-4773.
7. Kaushansky K. Historical review: megakaryopoiesis and thrombopoiesis. *Blood*. 2008;111:981-986.
8. Matsumura I, Kanakura Y. Molecular control of megakaryopoiesis and thrombopoiesis. *Int J Hematol*. 2002;75:473-483.
9. Kaushansky K. Thrombopoiesis. *Semin Hematol*. 2015;52:4-11.
10. Ulich TR, del Castillo J, Yin S, et al. Megakaryocyte growth and development factor ameliorates carboplatin-induced thrombocytopenia in mice. *Blood*. 1995;86:971-976.
11. Wolber EM, Jelkmann W. Thrombopoietin: the novel hepatic hormone. *News Physiol Sci*. 2002;17:6-10.
12. Zhang L, Xing D, Zhu DB, Chen Q. Low-power laser irradiation inhibiting A beta(25–35)-induced PC12 cell apoptosis via PKC activation. *Cell Physiol Biochem*. 2008;22:215-222.
13. Shefer G, Partridge TA, Heslop L, Gross JG, Oron U, Halevy O. Low-energy laser irradiation promotes the survival and cell cycle entry of skeletal muscle satellite cells. *J Cell Sci*. 2002;115:1461-1469.
14. Ozcelik O, Haytac MC, Kunin A, Seydaoglu G. Improved wound healing by low-level laser irradiation after gingivectomy operations: a controlled clinical pilot study. *J Clin Periodontol*. 2008;35:250-254.
15. Antunes HS, de Azevedo AM, Bouzas LFDS, et al. Low-power laser in the prevention of induced oral mucositis in bone marrow transplantation patients: a randomized trial. *Blood*. 2007;109:2250-2255.
16. Meng CB, He ZY, Xing D. Low-level laser therapy rescues dendrite atrophy via upregulating BDNF expression: implications for Alzheimer's disease. *J Neurosci*. 2013;33:13505-13517.
17. Zhang Z, Shen Q, Wu XL, Zhang D, Xing D. Activation of PKA/SIRT1 signaling pathway by photobiomodulation therapy reduces Abeta levels in Alzheimer's disease models. *Aging Cell*. 2020;19:e13054.
18. Zhang Q, Dong TT, Li PY, Wu MX. Noninvasive low-level laser therapy for thrombocytopenia. *Sci Transl Med*. 2016;8:349ra101.
19. Yang JK, Zhang Q, Li PY, Dong TT, Wu MX. Low-level light treatment ameliorates immune thrombocytopenia. *Sci Rep*. 2016;6:38238.
20. Arany PR, Cho A, Hunt TD, et al. Photoactivation of endogenous latent transforming growth factor-beta1 directs dental stem cell differentiation for regeneration. *Sci Transl Med*. 2014;6:238ra69.
21. Lu CX, Zhou FF, Wu SN, Liu L, Xing D. Phototherapy-induced antitumor immunity: long-term tumor suppression effects via photoinactivation of respiratory chain oxidase-triggered superoxide anion burst. *Antioxid Redox Signal*. 2016;24:249-262.
22. Matrosova VY, Orlovskaya IA, Serobyan N, Khaldoyanidi SK. Hyaluronic acid facilitates the recovery of hematopoiesis following 5-fluorouracil administration. *Stem Cells*. 2004;22:544-555.
23. Takano F, Tanaka T, Aoi J, Yahagi N, Fushiya S. Protective effect of (+)-catechin against 5-fluorouracil-induced myelosuppression in mice. *Toxicology*. 2004;201:133-142.
24. Yang RK, Miki K, He X, Killeen ME, Fink MP. Prolonged treatment with N-acetylcystine delays liver recovery from acetaminophen hepatotoxicity. *Crit Care*. 2009;13:R55.
25. Qi ZT, He Q, Ji L, Ding SZ. Antioxidant supplement inhibits skeletal muscle constitutive autophagy rather than fasting-induced autophagy in mice. *Oxid Med Cell Longev*. 2014;2014:315896.
26. Lu CX, Fan ZJ, Xing D. Photo-enhancement of macrophage phagocytic activity via Rac1-mediated signaling pathway: implications for bacterial infection. *Int J Biochem Cell Biol*. 2016;78:206-216.
27. Prislovsky A, Marathe B, Hosni A, et al. Rapid platelet turnover in WASP(-) mice correlates with increased ex vivo phagocytosis of opsonized WASP(-) platelets. *Exp Hematol*. 2008;36:609-623.
28. Lev PR, Goette NP, Glembotsky AC, et al. Production of functional platelet-like particles by the megakaryoblastic DAMI cell line provides a model for platelet biogenesis. *Platelets*. 2011;22:28-38.
29. O'Brien JJ, Spinelli SL, Tober J, et al. 15-deoxy-delta12,14-PGJ_2 enhances platelet production from megakaryocytes. *Blood*. 2008;112:4051-4060.
30. Ray DM, Spinelli SL, Pollock SJ, et al. Peroxisome proliferator-activated receptor gamma and retinoid X receptor transcription factors are released from activated human platelets and shed in microparticles. *Thromb Haemost*. 2008;100:86-95.
31. Avecilla ST, Hattori K, Heissig B, et al. Chemokine-mediated interaction of hematopoietic progenitors with the bone marrow vascular niche is required for thrombopoiesis. *Nat Med*. 2004;10:64-71.
32. Halene S, Gao Y, Hahn K, et al. Serum response factor is an essential transcription factor in megakaryocytic maturation. *Blood*. 2010;116:1942-1950.
33. Zhang ZZ, Liu L, Jiang XX, Zhai SD, Xing D. The essential role of Drp1 and its regulation by S-nitrosylation of parkin in dopaminergic neurodegeneration: implications for parkinson's disease. *Antioxid Redox Signal*. 2016;25:609-622.
34. Wheeler SE, Suzuki S, Thomas SM, et al. Epidermal growth factor receptor variant III mediates head and neck cancer cell invasion via STAT3 activation. *Oncogene*. 2010;29:5135-5145.
35. Liu J, Wang QC, Han J, Xiong B, Sun SC. Aflatoxin B1 is toxic to porcine oocyte maturation. *Mutagenesis*. 2015;30:527-535.
36. Hernandez-Garcia D, Wood CD, Castro-Obregon S, Covarrubias L. Reactive oxygen species: a radical role in development? *Free Radic Biol Med*. 2010;49:130-143.
37. Kojima S, Takaba K, Kimoto N, et al. Protective effects of glutathione on 5-fluorouracil-induced myelosuppression in mice. *Arch Toxicol*. 2003;77:285-790.
38. Reddy EC, Wang H, Annie Bang KW, Packham MA, Rand ML. Young steady-state rabbit platelets do not have an enhanced capacity to expose procoagulant phosphatidylserine. *Platelets*. 2018;29:27-33.
39. Sorensen AL, Rumjantseva V, Nayeb-Hashemi S, et al. Role of sialic acid for platelet life span: exposure of beta-galactose results in the rapid clearance of platelets from the circulation by asialoglycoprotein receptor-expressing liver macrophages and hepatocytes. *Blood*. 2009;114:1645-1654.
40. Kaushansky K, Lok S, Holly RD, et al. Promotion of megakaryocyte progenitor expansion and differentiation by the c-Mpl ligand thrombopoietin. *Nature*. 1994;369:568-571.
41. Wolber EM, Fandrey J, Frackowski U, Jelkmann W. Hepatic thrombopoietin mRNA is increased in acute inflammation. *Thromb Haemost*. 2001;86:1421-1424.
42. Grozovsky R, Begonja AJ, Liu K, et al. The Ashwell-Morell receptor regulates hepatic thrombopoietin production via JAK2-STAT3 signaling. *Nat Med*. 2015;21:47-54.
43. Hoffmeister KM, Falet H. Platelet clearance by the hepatic Ashwell-Morrell receptor: mechanisms and biological significance. *Thromb Res*. 2016;141:S68-S72.
44. Eichler M, Lavi R, Shainberg A, Lubart R. Flavins are source of visible-light-induced free radical formation in cells. *Lasers Surg Med*. 2005;37:314-319.
45. Carrasco E, Calvo MI, Blazquez-Castro A, et al. Photoactivation of ROS production in situ transiently activates cell proliferation in mouse skin and in the hair follicle stem cell niche promoting hair growth and wound healing. *J Invest Dermatol*. 2015;135:2611-2622.
46. Khuman J, Zhang J, Park J, Carroll JD, Donahue C, Whalen MJ. Low-level laser light therapy improves cognitive deficits and inhibits microglial activation after controlled cortical impact in mice. *J Neurotrauma*. 2012;29:408-417.
47. Bhat FA, Advani J, Khan AA, et al. A network map of thrombopoietin signaling. *J Cell Commun Signal*. 2018;12:737-743.
48. Wormann B. Clinical indications for thrombopoietin and thrombopoietin-receptor agonists. *Transfus Med Hemother*. 2013;40:319-325.
49. Chelsky ZL, Yue PB, Kondratyuk TP, et al. A resveratrol analogue promotes ERKMAPK-dependent Stat3 serine and tyrosine phosphorylation alterations and antitumor effects in vitro against human tumor cells. *Mol Pharmacol*. 2015;88:524-533.

50. Alexander L. Cyclic stretch induces fibronectin expression via c-Src- and STAT3-dependent pathways in renal epithelial cells. *FASEB J*. 2015;308:F425-436.
51. Pelicci G, Lanfrancone L, Grignani F, et al. A novel transforming protein (SHC) with an SH2 domain is implicated in mitogenic signal transduction. *Cell*. 1992;70:93-104.
52. Wang HT, Li SH, Li HL, et al. Grb2 interacts with SGEF and antagonizes the ability of SGEF to enhance EGF-induced ERK1/2 activation. *Mol Cell Biochem*. 2014;389:239-247.
53. Singh DK, Kumar D, Siddiqui Z, et al. The strength of receptor signaling is centrally controlled through a cooperative loop between Ca^{2+} and an oxidant signal. *Cell*. 2005;121:281-293.
54. Zhang JT, Xing D, Gao XJ. Low-power laser irradiation activates Src tyrosine kinase through reactive oxygen species-mediated signaling pathway. *J Cell Physiol*. 2010;217:518-528.
55. Giannoni E, Buricchi F, Raugei G, Ramponi G, Chiarugi P. Intracellular reactive oxygen species activate Src tyrosine kinase during cell adhesion and anchorage-dependent cell growth. *Mol Cell Biol*. 2005;25:6391-6403.
56. Fang YW, Han SI, Mitchell C, et al. Bile acids induce mitochondrial ROS, which promote activation of receptor tyrosine kinases and signaling pathways in rat hepatocytes. *Hepatology*. 2004;40:961-971.
57. Wu SN, Xing D, Wang F, Chen TS, Chen WR. Mechanistic study of apoptosis induced by high-fluence low-power laser irradiation using fluorescence imaging techniques. *J Biomed Opt*. 2007;12:064015.
58. Lavi R, Shainberg A, Friedmann H, et al. Low energy visible light induces reactive oxygen species generation and stimulates an increase of intracellular calcium concentration in cardiac cells. *J Biol Chem*. 2003;278:40917-40922.
59. Sun XG, Wu SN, Xing D. The reactive oxygen species-Src-Stat3 pathway provokes negative feedback inhibition of apoptosis induced by high-fluence low-power laser irradiation. *FEBS J*. 2010;277:4789-4802.

SUPPORTING INFORMATION

Additional supporting information may be found online in the Supporting Information section.

How to cite this article: Wang Q, Chang H, Shen Q, Li Y, Xing D. Photobiomodulation therapy for thrombocytopenia by upregulating thrombopoietin expression via the ROS-dependent Src/ERK/STAT3 signaling pathway. *J Thromb Haemost*. 2021;19:2029–2043. https://doi.org/10.1111/jth.15252